A GPU Computational Code for Eddy-Current Problems in Voxel-Based Anatomy

Published paper @DOI: 10.1109/TMAG.2014.2363140.

A GPU Computational Code for Eddy-Current Problems in Voxel-Based Anatomy

Oriano Bottauscio[1], Mario Chiampi[2], Jeff Hand[3] and Luca Zilberti[1]

[1] Istituto Nazionale di Ricerca Metrologica (INRIM), Torino (Italy)
[2] Dip. Energia, Politecnico di Torino, Torino (Italy)
[3] Division of Imaging Sciences and Biomedical Engineering, King's College London, London, UK

A hybrid Finite Element – Boundary Element method, developed to solve eddy current problems in the frequency-domain, is applied to the electromagnetic analysis of voxel based human models. A specific procedure employs a massively parallelized algorithm implemented on a multiple GPU code to speed up the solution of large systems whose matrix exceeds the RAM capability. The database structure used for the electromagnetic problem is also suitable for a successive thermal analysis to evaluate the distribution of the temperature elevation due to the energy deposited by the waves in the tissues. Finally, some examples of application are presented.

***Index Terms*— Biological effects of electromagnetic radiation, Magnetic resonance imaging, Eddy currents, Boundary Element Method, Finite Element Method.**

I. Introduction

The interest for the exposure of biological systems to electromagnetic fields (EMF) is more and more increasing due to the diffusion of EMF communication devices and diagnostic and therapeutic electromagnetic techniques, such as Magnetic Resonance Imaging (MRI). Numerical techniques, making use of anatomical human models associated to biological tissue properties (e.g. [1, 2]), have been developed for such a purpose. For the application in MRI dosimetry, the usual assumption of disregarding the magnetic field produced by currents induced within the body is acceptable only for relatively low-field scanners or exposure to gradient coil fields (e.g. [3-4]), while a general approach, where also the magnetic field is unknown (eddy current problem), is needed for the radiofrequency (RF) fields (e.g. [5-6]) or in presence of metallic implants [7-9].

This paper adopts a frequency domain T-ϕ formulation [10-11] for the computation of induced currents and energy deposition in a human body model. Temperature increase is consequently estimated by solving Pennes' bioheat equation [12]. Electromagnetic and thermal problems are solved by adopting the human body voxel structure as finite element (FE) mesh. A coupled Boundary Element (BE) technique prevents the domain truncation and the meshing of the air and field sources. A generalized minimal residual (GMRES) iterative solver [13] avoids the matrix storage, requiring the element recalculation at each iteration. The processing time is limited by implementing a massively parallelized algorithm on multiple GPUs, through the use of the Compute Unified Device Architecture (CUDA) platform and the Open Multiprocessing (OpenMP) libraries.

II. Field Formulations

A. Electromagnetic field problem

The 3-D domain Ω (human body) is characterized by a spatial distribution of the tissues properties (electrical conductivity σ and permittivity ε). The surrounding space (Ω_{ext}) with the field sources (coils with impressed current density) is nonconductive. All regions are nonmagnetic, with permeability μ_0.

The electromagnetic problem is formulated in the frequency domain (angular frequency ω), representing field quantities by phasors. The magnetic field $\mathbf{H} = \mathbf{H}_s + \mathbf{H}_i$ is decomposed into a primary field $\mathbf{H}_s$, produced by the sources in free space and evaluated through the Biot-Savart law, and a secondary field $\mathbf{H}_i$ generated by the total current density $\mathbf{J}$ (including conductive and displacement terms) induced in Ω. $\mathbf{J}$ is assumed to be bounded inside Ω, that is $\mathbf{J} = 0$ in Ω_{ext}.

The $\mathbf{T}$-ϕ formulation proposed in [11] is here adopted. A vector potential $\mathbf{T}$ ($\mathbf{J} = curl\mathbf{T}$ in Ω) and a scalar potential ϕ are introduced to describe the secondary field as $\mathbf{H}_i = \mathbf{T} + grad\phi$. The following field equations hold in Ω:

$$div\mathbf{T} + divgrad\phi = 0 \quad (1)$$

$$curl\left(\frac{1}{\tilde{\sigma}}curl\mathbf{T}\right) + j\omega\mu_0\mathbf{T} + j\omega\mu_0 grad\phi = -j\omega\mu_0\mathbf{H}_s \quad (2)$$

and the boundary condition $\mathbf{T} = 0$ over the body surface $\partial\Omega$, which implicitly imposes that induced currents are confined within the body. This condition also guarantees the uniqueness of ($\mathbf{T}$,ϕ), as proved in [11].

In the external open boundary domain Ω_{ext}, the Laplace

equation holds for ϕ, so that the following integral form holds:

$$\xi\phi + \int_{\partial\Omega} \left(grad\,\phi\cdot\mathbf{n}\right)^{(e)} \Psi ds - \int_{\partial\Omega} \phi\left(grad\,\Psi\cdot\mathbf{n}\right) ds = 0 \qquad (3)$$

where ξ is the singularity factor and $\Psi = 1/(4\pi r)$ and $\mathbf{n}$ is the outward normal unit vector.

Denoting by $\tilde{\sigma} = \sigma + j\omega\varepsilon$ the complex conductivity, the weak forms of (1) and (2), with test functions w and $\boldsymbol{\upsilon}$, are

$$\int_{\Omega} grad\,\phi\cdot grad w\, dv - \int_{\partial\Omega} w\, \left(grad\,\phi\cdot\mathbf{n}\right)^{(i)}\, ds + \int_{\Omega} \mathbf{T}\cdot grad w\, dv = 0 \qquad (4)$$

$$\int_{\Omega} \frac{1}{\tilde{\sigma}} curl\mathbf{T}\cdot curl\boldsymbol{\upsilon}\, dv + j\omega\mu_0 \left(\int_{\Omega} \mathbf{T}\cdot\boldsymbol{\upsilon}\, dv + \int_{\Omega} grad\,\phi\cdot\boldsymbol{\upsilon}\, dv \right) = = -j\omega\mu_0 \int_{\Omega} \mathbf{H}_s\cdot\boldsymbol{\upsilon}\, dv \qquad (5)$$

Continuity conditions on the magnetic flux density link internal (i) and external (e) quantities on the sides of $\partial\Omega$:

$$\left(grad\,\phi\cdot\mathbf{n}\right)^{(i)} = \left(grad\,\phi\cdot\mathbf{n}\right)^{(e)} \qquad (6)$$

The voxel structure in Ω is assumed as finite element mesh, introducing nodal shape functions and nodal unknowns (3-component vector $\mathbf{T}$ and scalar ϕ). The external faces of the voxels are used as boundary elements, assuming unknown $\left(grad\,\phi\cdot\mathbf{n}\right)^{(e)}$ uniform on each face; integral equation (2) is discretized adopting a collocation method where the source point is chosen in the barycenter of each face.

The power dissipated in each voxel is computed as $P_{em} = \Re\left(\mathbf{E}\cdot\mathbf{J}^{*}\right)/2$, where $\Re$ denotes the real part, E is the electric field ($\mathbf{J} = \tilde{\sigma}\mathbf{E}$) and **J*** is the conjugate of **J**; the Specific Absorption Rate (SAR) is then derived as P_{em}/δ, being δ the mass density of the tissue.

B. Thermal field problem

The thermal problem is analyzed under steady-state conditions through Pennes' bioheat equation [12], which models the thermal balance within human body. By introducing the temperature elevation $\theta(z) = \Theta(z) - \Theta_s(z)$ with respect to the temperature distribution before the exposure (Θ_s), the weak form of thermal equation becomes:

$$\int_{\Omega} \lambda\nabla\theta\cdot\nabla w dv + \int_{\Omega} h_b\theta w dv + \int_{\partial\Omega} h_{amb}\theta w ds = \int_{\Omega} P_{em} w dv \qquad (7)$$

where w is the shape functions associated to each voxel, P_{em} is the volume power density produced in the body by the electromagnetic field, λ is the thermal conductivity of tissues and h_b is the blood perfusion coefficient. The heat transfer towards the external environment is set by boundary conditions at the interface between body and air, through coefficient h_{amb}: $\partial\theta/\partial n|_{\partial\Omega} = \left(h_{amb}/\lambda\right)\theta$.

III. Computational Aspects

A. GPU implementation

Due to the large number of unknowns arising from the voxel datasets, the complex algebraic system is not stored in memory and a GMRES iterative algorithm is adopted to avoid matrix factorization. Since the matrix is not stored, only a diagonal preconditioner can be used for the GMRES algorithm. At each iteration, a matrix-vector product is performed by processing one matrix row at a time. The matrix row elements belonging to FE equations are computed on CPU, while the BE terms are computed by invoking parallel CUDA kernels; each thread performs the interactions among two elementary external surfaces, i.e. the integration of the Green function Ψ and its gradient. Due to limitations in the on-board global memory of GPU cards, the number of elements handled by the CUDA kernel is limited. For this reason, a set of CUDA kernels is sequentially invoked. The GMRES solution update is performed on CPU.

All computations have been performed on AMD Opteron 6276, 2.3 GHz, 16-cores server, in Windows HPC environment, using NVIDIA Tesla 2075 and Kepler K20 GPU cards. For each case, the elapsed time (i.e. the time interval from the start to the end of the program execution) for a single GMRES iteration is recorded, together with the number of computational elements handled by each GPU and the corresponding number of CUDA kernel calls. Both CPU and GPU algorithms have been optimized; in particular, CPU computations have been performed using the 16 cores of the AMD processor. We have not used fast-multiple type acceleration neither in the CPU nor in the GPU computations, so that the computational time are comparable.

The results in the simulation of a human head exposed to MRI RF field (see Section IV) are summarized in Table I, considering three voxel resolutions (5 mm, 3 mm and 1 mm) with increasing degree of freedom (DOF). All tests have been performed using double complex algebra. GPU speeds up simulations of a ratio ranging from 200 to 800, for the DOF here tested. Speed up is affected by the number of adopted GPUs and the card performances. The ratio between elapsed time and DOF (see last column in the Table), for a defined hardware configuration, are comparable.

B. Validation of computational code

The electromagnetic code has been previously validated by comparison with measurements carried out on a phantom,

TABLE I
COMPUTATIONAL DATA. THE ELAPSED TIME (Δ) IS NORMALIZED TO THE CASE WITH A VOXEL-SIZE OF 5 MM RUNNING ON KEPLER K20

Voxel size (mm)	*DOF* (10^6)	No. GPUs	GPU type	No.Element/ GPU	No. kernel calls	Δ (p.u.)	Δ/*DOF* (10^{-6}) (p.u.)
5	0.15	0	-	-	-	497	3310
		1	M2075	8800	1	2	13.3
		1	K20	8800	1	1	6.67
3	0.69	0	-	-	-	3910	5670
		1	M2075	8200	3	7.5	10.9
		1	K20	8300	3	4.5	6.52
1	18.7	0	-	-	-	$>10^5$	>6000
		1	M2075	1330	168	279	14.9
		2	M2075	1330	84	156	8.34
		4	M2075	1330	42	112	5.99
		1	K20	1200	188	197	10.5

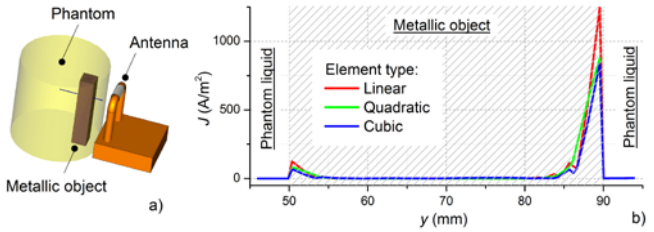

Fig. 1. Experimental set-up (a) and magnitude of the current density induced within a metallic object mimicking a passive bulk implant (b).

filled by a liquid with equivalent tissue properties (σ = 0.85 S/m, ε_r = 65) and radiated by a 64 MHz antenna (Fig. 1a), as reported in [14]. Thermal code was validated by comparison with the same analytical solutions used in [15].

Validation with experiments has been extended also in presence of highly conductive objects (implants) showing significant skin effect [14]. To avoid extremely low voxel size, higher-order finite element shape functions are adopted in the metallic parts. The effects of linear, quadratic and cubic Serendipity-type hexahedral elements [15] are compared in Fig. 1, which shows the spatial distribution of the current density induced in a metallic object (section equal to 40×40 mm^2, $\sigma = 1.35 \cdot 10^6$ S/m), placed inside a human phantom, to simulate a bulk passive prosthesis. The current density distribution within the metallic object, computed using 2 mm hexahedral elements, tends to settle moving from linear to cubic element types (see Fig. 1b).

IV. Application to MRI Dosimetry

Two exposure conditions in MRI environments are analyzed. In the first example, the spatial distribution of SAR and related temperature elevation are computed in a human head exposed to the RF field generated in 1.5 T and 3 T scanners (Fig. 2a). The second example focuses on the thermal effects produced by the RF field of a 1.5 T scanner in proximity of hip bilateral prostheses (Fig. 2b). In both cases, the antenna is a generic 16-rung bird-cage coil, similar to the body coils used in actual tomography. The source is assumed to be ideal, in that the currents flowing in the rungs and rings are not altered by the body, even if the local magnetic field within the body is modified. The reference frame is always

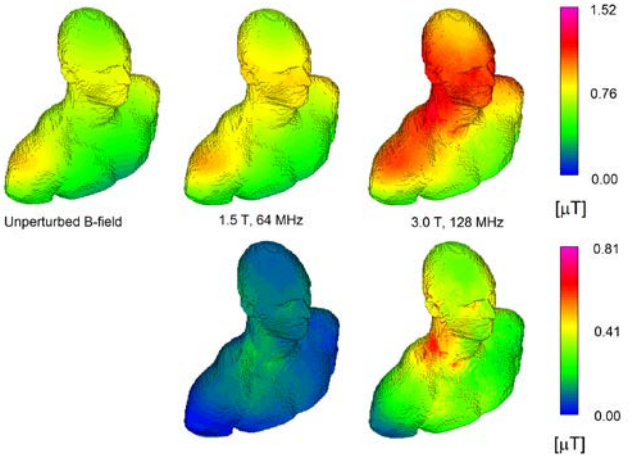

Fig. 4. In the upper figures, the B-field over the head surface: from left to right, the unperturbed field and the field at 64 MHz and 128 MHz. In the lower figures, the variation ΔB with respect to the unperturbed case.

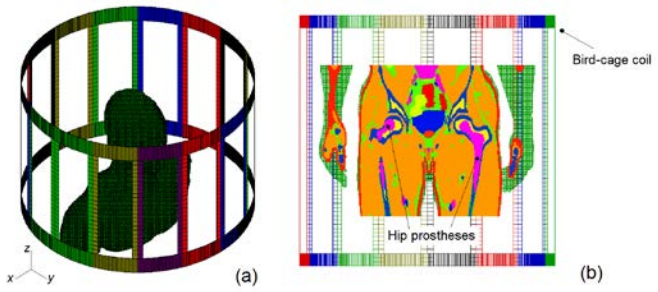

Fig. 2. Analyzed MRI exposures: (a) Head exposure at MRI, RF field at 64 MHz and 128 MHz; (b) Pelvis exposure with bilateral non symmetric hip prostheses (color represents the different tissues).

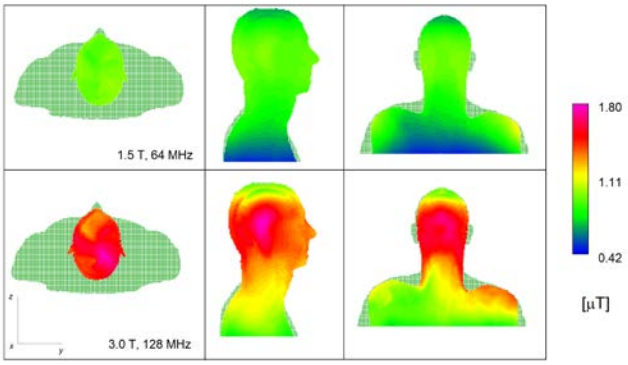

Fig. 3. Head exposure to RF MRI field. Local distribution of B-field for 64 MHz (upper) and 128 MHz (lower) in the transversal, sagittal and coronal sections (from left to right).

located at the isocenter of the bird-cage coil. The human model is the Duke dataset of the Virtual Family, with 77 tissues whose properties are taken from the IT'IS database [2].

Assuming an average MRI examination time of about 30 minutes and a typical tissue time constant of 6÷7 minutes, the thermal simulations can be performed under steady state conditions. Moreover, since during scanning sequences the RF is not continuously present for all the examination time, a duty cycle of 20% is here considered.

A. *Head exposure to RF field*

The head of the Duke model (3 mm-resolution) is placed within the bird-cage coil (diameter: 714 mm; height: 450 mm), as in Fig. 2a. To limit the computational time, the model is truncated at the shoulders, having preliminarily evaluated that results in the brain region are not significantly altered. The number of unknowns is ~2.6 10^6.

A 1 μT B_1^+ field is generated at the isocenter of the coil without the head. While at 64 MHz the magnetic flux density is almost unaltered by the body (Fig. 3), higher modifications occur at 128 MHz (maximum B-field up to 1.8 μT). The surface B-field is consequently modified, as shown in Fig. 4, which reports the RMS-value (this value could be monitored by a three-axial field probe) and its variation ΔB with respect to the unperturbed case. The maximum variation, at 128 MHz, is found in the neck region. Local SAR and steady-state temperature elevation in sagittal and coronal sections are shown in Figs. 5. Since the temperature elevation θ is strongly affected by the perfusion coefficient (relatively low in the neck region), there is not a direct spatial correlation between local values of SAR and θ. Adopting a RF duty cycle of 20%,

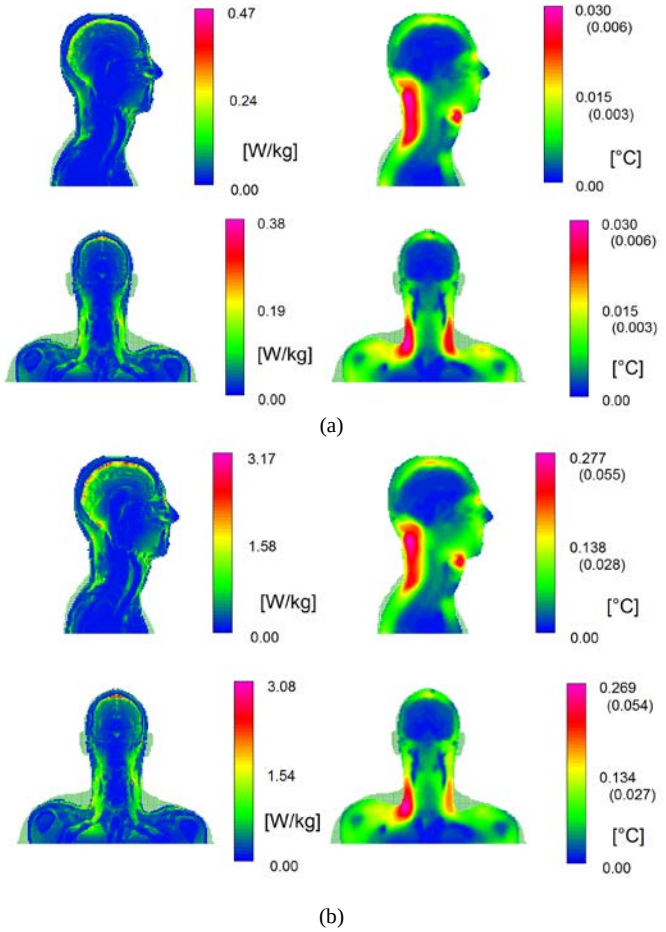

Fig. 5. Simulations at 64 MHz (a) and 128 MHz (b). From left to right, the local SAR and the temperature elevation in the sagittal section (upper) and in a coronal section (lower). Temperature elevations in brackets are rescaled with the RF duty cycle of 20%.

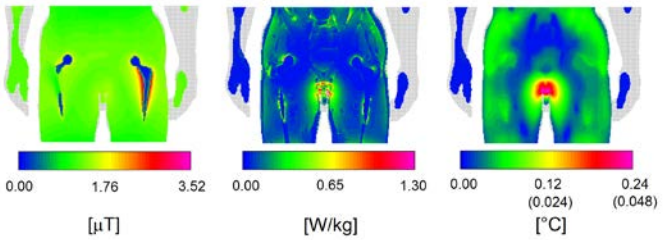

Fig. 6. Simulations at 64 MHz in presence of bilateral hip prosthesis. Spatial distribution of B-field (left), local SAR (centre) and temperature elevation (right) in a coronal section. Temperature elevations in brackets are rescaled with the RF duty cycle of 20%.

the maximum temperature elevations, for B_1^+ = 1 μT, are $6{\cdot}10^{-3}$ °C and $55{\cdot}10^{-3}$ °C at 64 MHz and 128 MHz, respectively. Values can be scaled to any B_1^+, since SAR and temperature elevation scales as $(B_1^+)^2$.

B. Body exposure in presence of hip-prostheses

In this analysis, the Duke model (2 mm-resolution) includes two hip prostheses (168 mm long and with a 24 mm diameter femoral head), inserted into the skeletal structure (bilateral implant). The prosthesis material (CoCrMo alloy) has electrical and thermal conductivities of $1.16{\cdot}10^6$ Sm^{-1} and 14 $Wm^{-1}°C^{-1}$, respectively. The position of the hips with respect to the 64 MHz, 16-rung bird-cage coil (diameter equal to 635 mm and height of 600 mm.) is shown in Fig. 2b. The model has been properly truncated without affecting the results around the implants, leading to a number of unknowns equal to ~10^7. The spatial distributions of B-field, local SAR and steady-state temperature elevation in a coronal section are reported in Fig. 6. The maximum temperature reached on the head of the hip prostheses, for B_1^+ = 1 μT, is ~0.1 °C, which reduces to $20{\cdot}10^{-3}$ °C applying a RF duty cycle of 20%.

V. Conclusions

The paper proposes and applies a numerical procedure to estimate the electromagnetic and thermal response of human tissues exposed in MRI environments. A hybrid FE-BE method employing a massively parallelized algorithm gives the distribution of the power deposited in the tissues, which acts as forcing terms for a successive FE solution of the thermal problem. Two scenarios (head exposed to RF radiation and effects of metallic bilateral hip prosthesis) are investigated to show the capabilities of the procedure.

Acknowledgment

This work was developed under the European Metrology Research Programme EMRP-HLT06 Joint Research Project (JRP) “Metrology for next-generation safety standards and equipment in MRI” (2012–2015). EMRP is jointly funded by the EMRP participating countries within EURAMET and the European Union. Funding was also received from the Italian MIUR project P7 “Metrology for therapeutic and diagnostic techniques based on electromagnetic radiation and ultrasound waves” (2014-2016).

References

[1] Virtual family, http://www.itis.ethz.ch/news-events/news/latest-news/
[2] P.A. Hasgall, E. Neufeld, M.C. Gosselin., A. Klingenböck, N. Kuster, “IT’IS Database for thermal and electromagnetic parameters of biological tissues,” Version 2.3, Feb. 2013. www.itis.ethz.ch/database
[3] M. Lu , S, Ueno, “Dosimetry of Exposure of Patients to Pulsed Gradient Magnetic Fields in MRI,” *IEEE Trans. Magn.*, Vol. 47, n. 10, pp. 1841-1844, 2011.
[4] O. Bottauscio, M. Chiampi, L. Zilberti, “Massively parallelized Boundary Element simulation of voxel-based human models exposed to MRI fields”, *IEEE Trans. Magn.*, Vol. 50, n. 2, pp. 7025504, 2014.
[5] J. Chi, F. Liu, L. Xia, T. Shao ; S. Crozier, “An Improved Cylindrical FDTD Algorithm and Its Application to Field-Tissue Interaction Study in MRI,” *IEEE Trans. Magn.*, Vol. 47, n. 2, pp. 466-470, 2011.
[6] A. Trakic, J. Jin, M.Y. Li, D. McClymont, E. Weber, F. Liu, S. Crozier, “A comparative numerical study of rotating and stationary RF coils in terms of flip angle and specific absorption rate for 7 T MRI,” *Journal of Magnetic Resonance*, Vol. 236, pp. 70-82, 2013
[7] S. Pisa, P. Bernardi, M. Cavagnaro, E. Piuzzi, “Power Absorption and Temperature Elevation Produced by Magnetic Resonance Apparatus in the Thorax of Patients With Implanted Pacemakers,” *IEEE Trans. Electromagnetic Compatibility*, Vol. 52, n. 1, pp. 32-40, 2010
[8] E. Mattei, G. Calcagnini, F. Censi, M. Triventi, P. Bartolini, “Numerical Model for Estimating RF-Induced Heating on a Pacemaker Implant During MRI: Experimental Validation,” *IEEE Trans. Biomed. Eng.*, Vol. 57, n. 8, pp. 2043-2052, 2010
[9] J. Powell, A. Papadaki, J. Hand, A. Hart, D. McRobbie, “Numerical Simulation of SAR Induced Around Co-Cr-Mo Hip Prostheses In Situ Exposed to RF Fields Associated with 1.5 and 3 T MRI Body Coils,” *Magnetic Resonance in Medicine* , Vol. 68, pp. 960–968, 2012.
[10] O. Biro, K. Preis, W. Renhart, G. Vrisk, K.R. Richter, “Computation of 3-D current driven skin effect problems using a current vector potential”, *IEEE Trans. Magn.*, Vol. 29, No. 2, pp. 1325-1328, 1993.

[11] M.R. Krakowski, “Some theorems of the eddy-current theory”, *Archiv für Elektrotechnik*, Vol. 74, pp. 329-334, 1991.
[12] Pennes H.H. “Analysis of tissue and arterial blood temperatures in the resting human forearm,” *Journal of Applied Physiology*, Vol.1, pp.:93–122, 1948.
[13] G. Borzì, O. Bottauscio, M. Chiampi, L. Zilberti, “Solution of Large Complex BEM Systems Derived from High-Resolution Human Models,” *IEEE Trans. Magn.*, Vol. 50, n. 2, pp. 7012804, 2014.
[14] D. Giordano, L: Zilberti, M. Borsero, M. Chiampi, O. Bottauscio, “Experimental validation of MRI dosimetric simulations in phantoms including metallic objects”. To appear on *IEEE Trans. Magn*.
[15] O. Bottauscio, M. Chiampi, L. Zilberti, “Boundary Element solution of electromagnetic and bioheat equations for the simulation of SAR and temperature increase in biological tissues”, *IEEE Trans. Magn*., Vol. 48, No. 2, 2012, pp. 691-694.
[16] M.V.K. Chari, S.J. Salon, Numerical methods in Electromagnetism, Academic Press, San Diego, 2000.